Single molecules of the bacterial actin MreB undergo directed treadmilling motion in *Caulobacter crescentus*

So Yeon Kim*, Zemer Gitai†, Anika Kinkhabwala*, Lucy Shapiro‡§, and W. E. Moerner*§

*Department of Chemistry, Stanford University, Stanford, CA 94305; †Department of Molecular Biology, Princeton University, Princeton, NJ 08544; and ‡Department of Developmental Biology, Beckman Center, Stanford University School of Medicine, Stanford, CA 94305

Contributed by Lucy Shapiro, June 2, 2006

The actin cytoskeleton represents a key regulator of multiple essential cellular functions in both eukaryotes and prokaryotes. In eukaryotes, these functions depend on the orchestrated dynamics of actin filament assembly and disassembly. However, the dynamics of the bacterial actin homolog MreB have yet to be examined *in vivo*. In this study, we observed the motion of single fluorescent MreB–yellow fluorescent protein fusions in living *Caulobacter* cells in a background of unlabeled MreB. With time-lapse imaging, polymerized MreB [filamentous MreB (fMreB)] and unpolymerized MreB [globular MreB (gMreB)] monomers could be distinguished: gMreB showed fast motion that was characteristic of Brownian diffusion, whereas the labeled molecules in fMreB displayed slow, directed motion. This directional movement of labeled MreB in the growing polymer provides an indication that, like actin, MreB monomers treadmill through MreB filaments by preferential polymerization at one filament end and depolymerization at the other filament end. From these data, we extract several characteristics of single MreB filaments, including that they are, on average, much shorter than the cell length and that the direction of their polarized assembly seems to be independent of the overall cellular polarity. Thus, MreB, like actin, exhibits treadmilling behavior *in vivo*, and the long MreB structures that have been visualized in multiple bacterial species seem to represent bundles of short filaments that lack a uniform global polarity.

bacteria | cytoskeleton | single-molecule fluorescence

In both eukaryotic and prokaryotic cells, actin mediates essential cellular processes. A quantitative understanding of the kinetic dynamics and ultrastructural architecture of actin's polymerized filaments has helped elucidate the mechanisms by which eukaryotic actin functions. For example, high-resolution imaging and the *in vivo* and *in vitro* dissection of the kinetics of its assembly have demonstrated how actin polymerization at the tips of a rigid, crosslinked actin meshwork can drive cell motility at the leading edge of *Dictyostelium* (1, 2). In budding yeast, the polarized assembly of actin cables provides both a road and direction signs for the directed transport of proteins to the tip of growing buds (3).

There are two known bacterial actin homologs, the widely conserved, chromosomally encoded MreB family of proteins and the plasmid-specific ParM family of proteins. ParM functions to partition plasmid DNA by polymerizing in between two sister plasmids, thereby generating a tension rod that physically pushes them apart (4). MreB is essential in most bacteria and has been shown to form a lengthwise spiral that contributes to cell shape, chromosome segregation, and polar protein localization in multiple species, including *Caulobacter crescentus*, *Escherichia coli*, and *Bacillus subtilis* (5–10). The mechanism by which MreB executes its functions remains largely unknown (11).

In vitro studies of the dynamics of eukaryotic actin filament assembly have demonstrated that actin polymerization is polarized such that ATP-bound monomers preferentially polymerize onto one filament end, hydrolyze their ATP to ADP while in the filament, and then preferentially depolymerize from the opposite filament end. Individual actin molecules thus appear to directionally flow, or treadmill, through seemingly stationary actin filaments (12–17). In contrast to actin's polarized assembly, the prokaryotic ParM protein polymerizes bidirectionally *in vitro* and exhibits dynamic instability with periods of constant growth interrupted by bursts of rapid depolymerization (18), a hallmark of eukaryotic tubulin (19). Although the polarity of MreB assembly has not been previously examined, initial *in vitro* studies with MreB from the extremophilic bacterium *Thermotoga maritima* have raised the possibility that the elongation of MreB polymers differs from actin, because MreB seems to require a lower protein concentration for spontaneous polymerization (critical concentration) and can polymerize in the presence of either ATP or GTP (20, 21).

When carefully examined, the quantitative dynamics of eukaryotic actin assembly *in vivo* and *in vitro* have often differed. The finding that the rate of actin depolymerization was far greater *in vivo* than *in vitro* actually led to the prediction of the existence of actin depolymerization factors and to the eventual identification of actin depolymerizing factor/cofilin (22). Thus, we sought to develop an *in vivo* method for characterizing the assembly kinetics of MreB. We specifically focused on *C. crescentus*, because *Caulobacter* MreB is essential and regulates cell morphology, chromosome segregation, and polar protein localization (8–10). *Caulobacter* also has an inherently asymmetric life cycle: With each cell cycle, it constructs a cellular extension (known as a stalk) at one pole of the cell [stalked (ST) pole] and a flagellum at the opposite pole (swarmer pole), such that division gives rise to two daughter cells that differ in polar morphology, size, and cell fate (23). With each cell cycle, *Caulobacter* MreB forms a dynamic spiral that condenses into a ring positioned at the future division plane and then expands back into a lengthwise spiral (8).

In this study, we use quantitative imaging of single- molecule fluorescence to assess the dynamics of MreB fused to a fluorescent protein in living *Caulobacter* cells. Single-molecule imaging of fluorescent protein fusions has been successfully applied to various living cells to study intracellular dynamics (24–27). This method allows classification of MreB–yellow fluorescent protein (YFP) motion into both polymerized and unpolymerized populations. Unpolymerized monomers move rapidly in a random walk but appear to have a restricted rate of diffusion compared with cytoplasmic proteins. By analyzing the rate, distance, and direction of polymerized monomer motion, we were able to demonstrate that MreB filaments indeed treadmill

Conflict of interest statement: No conflicts declared.

Abbreviations: fMreB, filamentous MreB; gMreB, globular MreB; YFP, yellow fluorescent protein; MSD, mean square displacement; ST, stalked.

§To whom correspondence may be addressed. E-mail: shapiro@stanford.edu or wmoerner@stanford.edu.

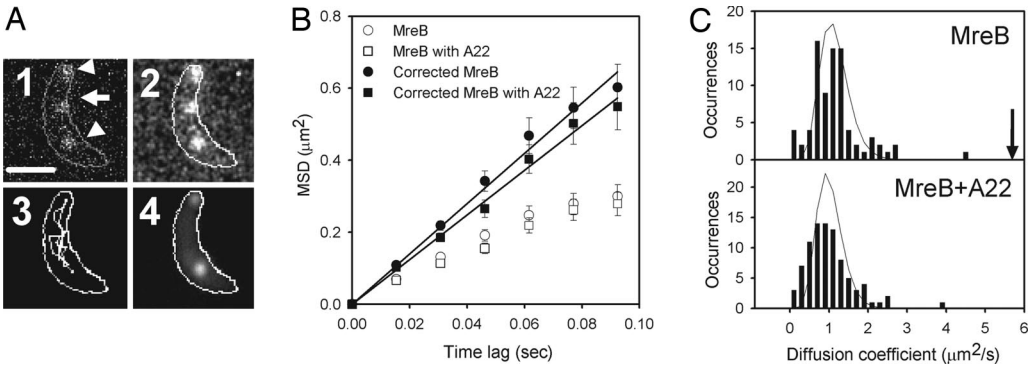

Fig. 1. Unpolymerized single MreB–enhanced YFP molecules exhibit random motion. (*A*) Fluorescence images of single MreB–YFP proteins in a *Caulobacter* cell. White line shows the cell outline. (*A1*) Image showing three fluorescent molecules (MreB–YFP) in a cell at 15.4-ms integration time. The top and bottom molecules are stationary; the middle molecule is moving. (*A2*) Smoothed image of *A1* obtained by applying a low-pass filter (3 × 3 kernels of 0.0625, 0.125, 0.0625, 0.125, 0.25, 0.125, 0.0625, 0.125, and 0.0625). (*A3*) A representative trajectory of the mobile molecule (middle spot in *A1*). (*A4*) Summed image of 450 sequential images. The fluorescence from the two stationary molecules is evident, whereas the middle molecule does not appear. (Scale bar, 1 μm.) (*B*) MSD of fast-moving MreB molecules versus time lag for both untreated and A22-treated cells (open circles and squares), with geometry-corrected data shown as filled circles and squares. Solid lines represent a linear fit of the corrected data. (*C*) Distributions of diffusion coefficients from individual molecules, from trajectories truncated to 10 time steps. MreB, $n = 81$; MreB + A22, $n = 84$. Solid lines represent the error distribution (39), assuming a homogeneous underlying diffusion coefficient. The arrow shows the expected diffusion coefficient of MreB (62 kDa) in cytoplasm.

in vivo and thus assemble in a kinetically polarized fashion. From these data, we also extracted the average MreB filament length and the direction of its polarity with respect to the long axis of the cell. Together, these results demonstrate that, in living cells, MreB assembles in a manner similar to that of its eukaryotic actin homolog, establishing the basis for understanding the assembly, organization, and function of this central regulator of bacterial cell biology.

Results

Single MreB–YFP Molecules Can Be Observed *in Vivo*. To observe MreB dynamics *in vivo*, we used single-molecule fluorescence imaging of a fusion of MreB to YFP (MreB–YFP). Because this method depended on the presence of a small number of MreB–YFP molecules per cell, we constructed a merodiploid *Caulobacter* strain containing a wild-type, unlabeled copy of MreB under its endogenous promoter as well as a single copy of a xylose-inducible MreB–YFP fusion integrated at the *PxylX* locus (28). This strain was treated with varying concentrations of xylose to find the optimal induction level for single-molecule visualization. With 0.0006% xylose (1X), a *Caulobacter* cell typically showed three to four discrete fluorescent molecules that could be easily resolved from one another (Fig. 1*A1*; see also Movie 1, which is published as supporting information on the PNAS web site). To visualize the fluorescent molecules more clearly, a smoothed version of the image was generated by low-pass spatial filtering, as shown in Fig. 1*A2*. Several assays confirmed that these fluorescent spots represent single MreB molecules and not aggregates. The fluorescence signals showed single-step digital photobleaching and the clear on–off blinking behavior that is characteristic of single molecules (29) (see Fig. 4, which is published as supporting information on the PNAS web site). In addition, the number of detected photons from a single MreB–YFP before photobleaching (≈91,000) was comparable to the literature value for single YFP molecules (≈140,000) (30) (data not shown). The fluorescent spots that we observed did not appear to be free YFP that had been cleaved from MreB, because the size of the fluorescent spot was comparable to that of a diffraction-limited spot (≈240 nm in diameter), whereas the rapid motion of the smaller free YFP protein caused it to appear as a larger diffuse object, even on the 15.4-ms timescale (diffusion coefficient of ≈7.7 $\mu m^2/s$) (31). Thus, multiple criteria support the conclusion that we have observed the fluorescence of single MreB–YFP molecules.

Polymerized and Unpolymerized MreB Can Be Distinctly Visualized as Two Separate Populations. With rapid continuous irradiation and detection (65 frames per s, 15.4-ms integration per frame, and total time of ≈7 s), we observed two different classes of behavior for single MreB–YFP molecules. Some of the molecules moved rapidly to many locations, whereas others appeared to be essentially stationary on this timescale. In Fig. 1*A1*, the arrow points to a mobile molecule, and the arrowheads point to molecules that are stationary during the total observation time. The observed trajectory of the mobile molecule is shown in Fig. 1*A3* as a white line. To contrast the two populations more clearly, we summed all 450 images pixel by pixel (Fig. 1*A4*); the spots from both the top and bottom molecules are visible because they were not mobile, whereas the spot from the middle (mobile) molecule disappears. Because MreB is an actin homolog that can polymerize *in vitro* into filaments in the presence of ATP (32), we hypothesized that the stationary molecules represent MreB proteins whose diffusions are constrained by being assembled into an extended polymer [filamentous MreB (fMreB)], whereas the mobile molecules represent free, unpolymerized MreB proteins [globular MreB (gMreB)]. To test this hypothesis, we treated cells with A22 (33). A small-molecule chemical inhibitor of MreB function (9), A22 is thought to interact directly with the MreB ATP-binding pocket, leading to disruption of MreB filaments and consequently diffuse MreB–YFP fluorescence (9); moreover, A22 perturbs the *in vitro* polymerization of an archaeal MreB homolog (34). When cells were incubated with 10 μg/ml A22, stationary molecules were not observed (see Movie 2, which is published as supporting information on the PNAS web site). However, fast, mobile spots were observed regardless of the A22 treatment. Because the disruption of MreB filaments specifically abolishes the stationary form of MreB–YFP single molecules, we conclude that the stationary and mobile MreB populations that are observed at rapid timescales indeed represent polymerized fMreB and unpolymerized gMreB, respectively.

Analysis of the Motion of gMreB. The ability to discriminate between fMreB and gMreB afforded us the capability to directly examine the dynamics of each population. To characterize the

behavior of the fast, mobile molecules, individual molecules were tracked by recording their center position as a function of time. One hundred eleven trajectories were obtained from untreated cells (30 individual cells), and 132 trajectories (27 individual cells) were obtained for A22-treated cells. We tracked each molecule until it disappeared (although it is possible that we tracked one molecule several times because of the blinking behavior of the YFP).

The observed mean square displacements (MSDs) as a function of time lag (Δt) for pooled data are shown in Fig. 1*B* (open symbols). Even though the curve departs from linearity at long times (considered below), we can extract an approximate diffusion coefficient D from the slope of the MSD plot by using the first four points. The D values were 1.11 ± 0.18 $\mu m^2/s$ and 0.95 ± 0.14 $\mu m^2/s$ in the absence or presence of A22, respectively, exhibiting no significant difference. These values are much smaller than the D value of 5.83 $\mu m^2/s$ that is expected for a cytoplasmic protein with the mass of MreB–YFP (62 kDa), as estimated from D for cytoplasmic GFP (27 kDa; $D = 7.7\ \mu m^2/s$) (31), assuming a simple $(mass)^{-1/3}$ scaling of the hydrodynamic radius. The fact that gMreB does not diffuse like a cytoplasmic protein suggests that it may associate with an additional factor(s).

An attractive explanation for the slower than expected movement of gMreB and the curvature of MSD versus time lag is that MreB associates with the plasma membrane. MreB has been shown to biochemically associate with the *Caulobacter* membrane (10), although it was not determined whether the membrane-associated protein represented polymerized or unpolymerized MreB. To explore the possibility that membrane association affects our measured diffusion coefficient, we modeled MreB movement as a membrane-bound particle, taking into account the capped-tube shape of the *Caulobacter* cell. As described in detail in ref. 25, a simulation of 3D diffusional movement on the cell surface allows correction of the MSD values so that they apply to true 2D diffusion, effectively flattening the cell into a plane (Fig. 1*B*, closed symbols). Using this approach, we extracted corrected D values in the absence or presence of A22 as 1.75 ± 0.17 $\mu m^2/s$ and 1.55 ± 0.16 $\mu m^2/s$, respectively. These values are consistent with observed D values for membrane-bound proteins reported by others (26). Therefore, it seems reasonable that membrane association could contribute to our observed movement of gMreB.

To determine whether gMreB exhibits homogeneous diffusion properties, distributions of measured diffusion coefficients from individual molecule trajectories at a time lag of 15.4 ms were examined for both untreated and A22 treated cells (Fig. 1*C*). The average diffusion coefficient was 1.15 ± 0.05 $\mu m^2/s$ for untreated MreB ($n = 81$) and 1.03 ± 0.04 $\mu m^2/s$ for A22 treated MreB ($n = 84$), comparable to the uncorrected diffusion coefficients. The agreement between the data and the expected error distribution (smooth curve) (35) shows no evidence for heterogeneity.

Polymerized MreB Molecules Undergo Directional Movement. Although the fMreB molecules did not appear to move on the timescale of a few seconds with continuous imaging, we used time-lapse imaging to explore the possibility that they might be moving over a longer timescale. Different dark intervals (0.9, 4.9, and 9.9 s) were inserted between acquisitions of fluorescence images (100-ms exposure). By reducing photobleaching, this time-lapse imaging allowed observation of the behavior for a longer period than would normally be possible. We were easily able to observe clear directional motion of fMreB molecules with 9.9-s dark intervals (Fig. 2*A*; see also Movies 3 and 4, which are published as supporting information on the PNAS web site). Motion of the entire cell was ruled out by observation of the diffuse fluorescence from the fast-moving gMreB. Even though

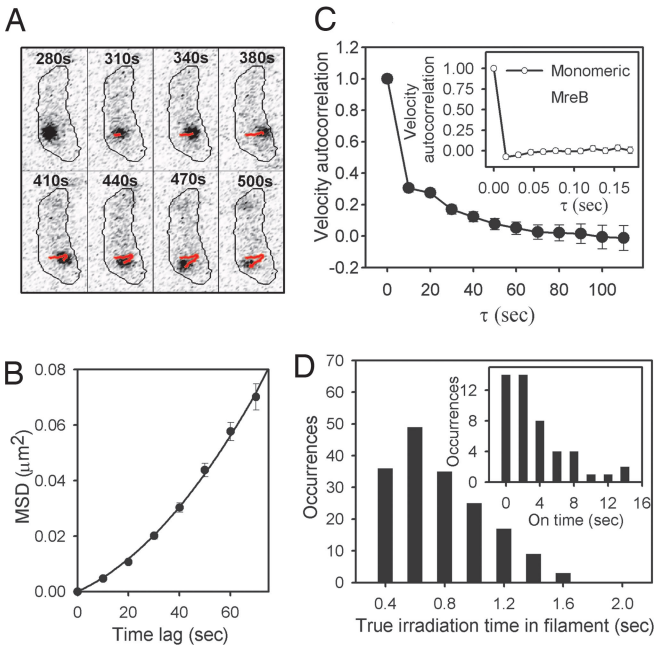

Fig. 2. Polymerized single MreB-enhanced YFP molecules exhibit directed motion consistent with treadmilling. (*A*) Fluorescence images illustrating the directional movement of fMreB. Time-lapse imaging with 10-s dark intervals, 100-ms exposures, black line showing the cell outline, and inverted contrast. The molecule moves from left to right and then turns and moves right to left at a downward angle, shown by the red line. (*B*) MSD versus time lag for fMreB with a quadratic fit (smooth line), indicative of directional motion. (*C*) Velocity autocorrelation for both gMreB (*Inset*) and fMreB. The autocorrelation of gMreB dropped to near zero at the very first time lag, whereas that for fMreB remained positive over at least 80 s. (*D*) Distribution of observed true irradiation time of fMreB molecules. *Inset* shows the distribution of total emission times before photobleaching of fMreB–YFP with continuous illumination (100-ms integration). Although the average ''on'' time of the fluorophore was 4.6 s (*Inset*), the average irradiation time of fMreB in the time-lapse experiment was 0.8 s.

the depth of focus was ≈350 nm and the average cell thickness was ≈430 nm, in a few cases, we could observe the molecules moving in a zigzag motion (the same molecule moved across the cell and then back) (Figs. 2*A* and 3*C*). This movement is reminiscent of the known helical distribution of *Caulobacter* MreB filaments, which further suggests that the slow MreB molecules are incorporated into polymerized filaments.

To quantify this motion, MSD values as a function of time lag were calculated (Fig. 2*B*). We analyzed 120 of 174 trajectories, because some of the molecular positions could not be fit to a 2D Gaussian function because of the blinking of YFP. The plot of the MSD of a particle moving in one direction is characterized by a quadratic dependence on time lag (36–38), and our MSD of polymerized MreB followed this behavior. The vertical scale in Fig. 2*B* shows that the slowly moving molecules did not move nearly as far as the monomers discussed above, such that nonideal behavior due to the nonplanar cell shape has less effect here. Nevertheless, to guard against this concern, only separate linear portions of the zigzag trajectories were included in the final analysis. The speed of polymerized MreB motion was computed to be 2.9 ± 0.1 nm/s by using a fit to the equation $MSD = 4Dt + (Vt)^2$, where D is the diffusion coefficient and V is the speed.

Another way to verify directional motion is to calculate the velocity autocorrelation function $C_V(\tau)$ (39–41). For a random walk, $C_V(\tau)$ simply drops to zero at the very first time step. However, a directed mover should have positive nonzero correlation due to the tendency to keep moving in the same direction as before. Fig.

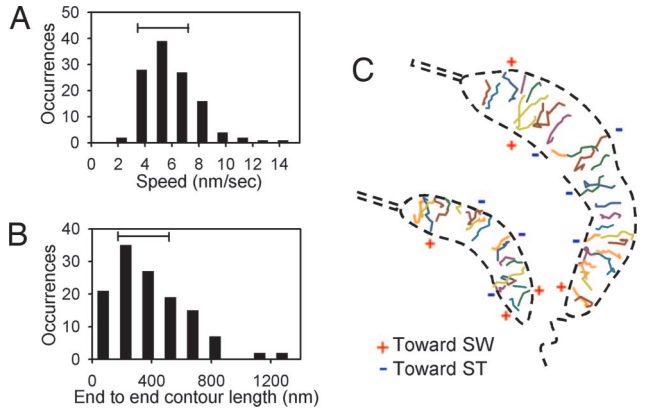

Fig. 3. *In vivo* assessment of MreB polymer assembly rate, length, and polarity. (*A*) Speed distribution of polymerized fMreB. The average speed was 6.0 ± 0.2 nm/s. (*B*) Distribution of end-to-end contour lengths measured from the movement of a single fMreB. The average length was 332 nm, which was quite small compared with the average cell length (3.5 μm). (*C*) Representative trajectories of fMreB filaments in a ST cell and in a predivisional cell. The single-molecule trajectories were plotted on normalized cell shapes as described in *Supporting Text*. Examples of global direction assignments are shown as either ''+'' [toward the swarmer (SW) pole] or ''−'' (toward the ST pole).

2*C* shows the measured $C_V(\tau)$ for gMreB and fMreB. gMreB shows a drop of correlation to near zero at the first time step (Fig. 2*C Inset*), whereas fMreB has positive correlation until $\tau = 80$ s. This timescale is consistent with the MSD analysis as well as the average number of frames (approximately eight, discussed below) for which we could observe fMreB molecules. Even though the autocorrelation of fMreB dropped significantly at the first time lag of 10 s, this drop can be explained by the fact that we conservatively recorded the same position twice (i.e., zero velocity) when we saw any blinking behavior. Together, these data demonstrate that gMreB follows a fast random walk and that fMreB exhibits slow, directed motion.

MreB Monomers Exhibit Treadmilling Through Short Filaments *in Vivo*. There are two possible explanations for the directional movement of fMreB: Either the filaments into which these monomers are incorporated are moving, or the monomers themselves are treadmilling through largely stationary filaments. The latter treadmilling motion is plausible because of the structural and kinetic similarities between MreB and actin. Actin's well documented treadmilling behavior results from polarized assembly wherein monomers are preferentially polymerized on one filament end and depolymerized from the other filament end. Such polarized assembly or treadmilling has yet to be documented for MreB *in vitro* or *in vivo*.

If the motion of fMreB is due to whole-filament movement, then the observation time for fMreB single molecules should be limited by only the photobleaching rate of the YFP and should thus be the same regardless of the experiment's timescale. In contrast, the observation times for monomers undergoing treadmilling motion should be limited by both photobleaching and depolymerization from the filament end. To quantify the photobleaching component, single molecules were observed with continuous illumination until emission ceased for a long time (photobleaching), ignoring short (one to two frame) blinking events. The average emission time of single polymerized MreB molecules was 4.6 s with continuous illumination (Fig. 2*D Inset*). This average emission time under continuous illumination should be compared with the distribution of true irradiation times for the time-lapse experiments (10-s dark periods between 100-ms acquisitions), which have a mean length of 0.8 s (Fig. 2*D*). With these statistics, we concluded that most of the fluorescence from the polymerized MreB molecules disappeared before they photobleached, likely as a result of dissociation from the end of the filament and onset of diffusive motion. These results argue in favor of MreB molecule treadmilling through filaments with fixed ends. Consequently, MreB appears to resemble actin not only in structure but also in assembly dynamics.

***In Vivo* Assessment of Average MreB Polymerization Rates and Filament Lengths.** Given that single fMreB molecules exhibit directed motion, a speed value was extracted from each single-molecule trajectory. The speed distribution for individual molecules is shown in Fig. 3*A*. The average speed was 6.0 ± 0.2 nm/s (n = 120, SEM). The slight difference between the average speed value and the quadratic fit in Fig. 2*B* is likely due to small changes in direction during each trajectory. The error bar on the figure shows the error of determination of any one speed; therefore, the excess width of the measured distribution suggests the presence of heterogeneity.

We were able to estimate the steady-state rate of MreB monomer polymerization and depolymerization by combining treadmilling speed measurements with the known structural dimensions of MreB. The monomer length of the MreB molecule from its crystal structure is 5.4 nm (32); in steady-state fixed filaments, addition of each monomer at one end is accompanied by release of a monomer at the other end. Thus, our observed speed of 6.0 nm/s can be converted to a steady-state rate of monomer addition of 1.2 s^{-1}.

The other physical property that can be extracted from our treadmilling observations is the average length of the MreB polymer filaments. With a fixed steady-state treadmilling filament, the total distance a molecule travels from the time it polymerizes until the time it dissociates can be regarded as the length of the polymer filament. We extracted the distribution of the end-to-end contour length from our trajectories as shown in Fig. 3*B*, using only newly polymerized molecules (that is, molecules that appeared as spots after the start of imaging). The average MreB filament length is 392 ± 23 nm (n = 128, SEM). The error bars in Fig. 3 are the SDs of the distributions, which estimate the error of single measurements. The observed average filament length is quite small compared with average cell length (3.5 μm), suggesting that the extended MreB helical structure reported previously may be composed of multiple short filaments rather than a few long filaments. It is plausible that by observing only ST and predivisional cells (see Fig. 5, which is published as supporting information on the PNAS web site), we are sensing primarily the time in the cell cycle when the helix is converting from an extended form (ST state) to a ring at the divisional plane and when the new helix is not fully formed (predivisional state). Because of the depth of focus, it is also possible that we could not observe the entire trajectory in every case, especially when the molecule moved along the cell edge and went beyond the edges of the focal plane. However, most of the traces showing zigzag motions have a similar length regardless of where they started, and many of the molecules moved less than the distance from one edge of the cell to the other edge (Fig. 3*C*).

Individual Filaments Appear to Grow in a Direction Independent of the Global Cell Polarity. Treadmilling filaments are inherently polarized, with a growing end and an end that shortens. Having established that MreB treadmills, we take the direction of single-molecule spot motion to indicate the local MreB filament polarity. *Caulobacter* cells are polarized, most notably evidenced by the presence of a stalk at one pole, and we calculated that the average MreB filament length is quite short relative to the total cell length. Thus, we were curious to see whether the multiple filaments that must constitute the overall MreB helix have a reproducible polarity with respect to the global cell polarity.

To show the overall behavior more clearly, we projected some of the trajectories from single polymerized MreB molecules onto a normalized cell shape (colored lines in Fig. 3*C*; the method is described in *Supporting Text*, which is published as supporting information on the PNAS web site). Surprisingly, most of the trajectories moved perpendicular to the cell long axis, along a radius of the circle, and thus cannot be said to be oriented toward either pole. A relatively small number of the trajectories showed oblique lines and zigzag shapes. To quantify the analysis for all trajectories, a well defined procedure was used to determine whether a polarized filament was oriented toward or away from the ST end of the cell (see *Supporting Text* and Fig. 6, which is published as supporting information on the PNAS web site). The plus and minus labels in Fig. 3*C* show a few examples of this determination. The results of this analysis yielded no significant preference for local filament orientation toward or away from the ST pole (see Table 1, which is published as supporting information on the PNAS web site). In other words, the short polymerized MreB segments have a polarity that seems to be random relative to the overall cell polarity.

Discussion

The actin homolog MreB has been shown to be essential for cell viability, cell shape, polar protein localization, and chromosome segregation in a wide array of bacterial species (5–10). These central functions of MreB are thought to depend on its dynamic ability to polymerize into filaments. In this study, we extend our understanding of MreB assembly and function by reporting the dynamic motion of single molecules of both gMreB and fMreB populations in living *Caulobacter* cells.

Unpolymerized MreB Does Not Behave Like a Free Cytoplasmic Protein. Surprisingly, the diffusion coefficient that we calculated for the unpolymerized MreB form was significantly slower than expected for a free cytoplasmic protein of similar size. Such slower diffusion indicates the presence of an as yet uncharacterized force that restricts the movement of unpolymerized MreB. Our modeling suggests that the slower diffusion could be explained by the association of unpolymerized MreB with the cell membrane. Although polymerized MreB filaments are found directly under the membrane and bulk MreB sediments in the membrane-associated cell fraction (10), the MreB protein sequence does not bear any motifs that are indicative of membrane association. It will prove interesting to determine whether unpolymerized MreB has an inherent affinity for the phospholipid membrane or for specific membrane-bound proteins. Alternatively, it remains a possibility that unpolymerized MreB is not membrane-associated but instead interacts with a larger protein complex that could function to sequester MreB or exchange its nucleotide, much as CAP (cyclase-associated protein) or profilin function for eukaryotic actin (42).

MreB Assembles in a Polarized Fashion *in Vivo*. By observing the behavior of polymerized MreB molecules, we were able to assess several parameters of the *in vivo* assembly of MreB filaments. We determined that polymerized MreB molecules move in a directional manner and, by comparing their on-time persistence, determined that this directed motion is likely to reflect treadmilling of monomers through filaments (with fixed ends), rather than wholesale filament translocation. The directed motion also argues against the possibilities that filament segments might be coming loose or that the filaments are coiling up and reannealing. This treadmilling behavior appears qualitatively similar to eukaryotic actin treadmilling that has been reported both *in vitro* (12–14, 43) and *in vivo* (15–17). The rate of monomer motion also allowed us to calculate the steady-state rate of MreB treadmilling to be 1.2 s^{-1}. At steady state, the rate-limiting step of actin treadmilling has been shown to reflect the rate of monomer dissociation from the pointed end. The range of actin treadmilling rates is reported to be 0.2–0.9 s^{-1} *in vitro*, similar to MreB's *in vivo* treadmilling rates. In different contexts, 10- to 100-fold increases in the actin treadmilling rate could be observed *in vivo* with the help of accessory proteins such as actin depolymerizing factor/cofilin (22). This discrepancy between the *in vivo* actin and MreB treadmilling rates could reflect either the absence of an MreB depolymerization factor in *Caulobacter* or inherent differences between actin and MreB polymerization. It is also formally possible that the fusion of MreB to YFP affects its dynamics, although the extremely low levels of MreB–YFP expression used in this study make such effects unlikely. Interestingly, another bacterial actin homolog, the plasmid-encoded ParM protein, exhibits bidirectional, rather than polarized, filament assembly (18). ParM functions by symmetrically extending from the cell center toward the two poles, whereas both actin and MreB are involved in localizing asymmetrically distributed macromolecules. Thus, polarized treadmilling may not be an inherent feature of actin-like filaments; instead, it may reflect the involvement of a filament in polarized processes.

Models for the Intracellular Organization and Activity of MreB. We were able to explore additional aspects of the ultrastructural organization of MreB filaments by quantitating several aspects of the motion of polymerized MreB molecules. The distance traveled by each polymerized MreB molecule allowed us to model the average filament length, which we estimate to be ≈400 nm. MreB spiral structures have been observed traversing the cell from pole to pole for lengths of several microns by both ensemble imaging of GFP fusions and immunofluorescence (8, 10, 44, 45, 49). The fact that we found individual filaments to be significantly shorter than the overall MreB spiral suggests that MreB spirals consist of multiple small filaments that are bundled together.

MreB has been shown to be a determinant of polar protein localization and the translocation of chromosomal origins toward cell poles in both *Caulobacter* and *E. coli* (6, 9, 46, 47), leading to the hypothesis that MreB structures possess a uniform polarity that can be interpreted by trafficking factors. However, by using the direction of treadmilling as an assay for the polarity of individual MreB filaments, we find a roughly even distribution of filaments directed toward either pole in every cell type and cell compartment examined. This heterogeneous filament polarity could indicate that the overall MreB spiral does not have a uniform polarity. Because it is difficult to understand how MreB could lead to directed macromolecular trafficking in this scenario, such a model would support less directed models for MreB's involvement in such processes. Alternatively, the heterogeneous filament polarity could reflect the presence of two separate spirals or a continuous "closed track" spiral, wherein each MreB bundle has a uniform polarity but there exist bundles of both polarities in each cell, allowing for directed trafficking to each pole. Higher resolution imaging (by cryoelectron tomography, for example) should allow these possibilities to be distinguished.

In this study, we have provided evidence that MreB spirals consist of bundles of multiple short filaments that each assemble in a polarized manner. The similarities between MreB and actin are thus kinetic as well as structural. This work should establish a constructive framework for future efforts exploring the factors that interact with MreB to influence its assembly and function as well as its detailed, high-resolution architecture.

Materials and Methods

Bacterial Strains and Plasmid. A xylose-inducible, YFP-labeled MreB fusion was introduced in single copy into the *Caulobacter* chromosome to tightly control the expression of this fluorescent fusion protein. The required *Pxyl:efyp-mreB* plasmid was prepared as described in ref. 8. Importantly, these N-terminal YFP-fused

MreB cells recapitulated the localization pattern of the endogenous MreB (10), and similar fusions to MreB homologs were functional in other bacterial systems (48, 49). The movement of cytoplasmic YFP proteins was observed with the previously described EJ153 strain (50). Both MreB–YFP and cytoplasmic YFP were induced by the addition of xylose to the media.

Sample Preparation. Cells were grown overnight in PYE media at 30°C and then diluted into M2G minimal media with specific concentrations of xylose (51). After the cells reached their logarithmic growth phase, cells were harvested by gentle centrifugation, added to a 1.5% agarose (A-0169, Sigma) pad slide along with 1 μl of a quantum dot solution (10 nM Qdot 565; Quantum Dot Corporation, Carlsbad, CA), and covered with a coverslip for room-temperature imaging as described in ref. 25. The quantum dots were later used as fiduciary markers. Different xylose concentrations were used for the following experiments: (*i*) to track monomeric MreB–YFP molecules, the cells were grown in 0.0006% xylose (1X); (*ii*) cytoplasmic YFP in EJ153 was induced with 0.006% xylose (10X); (*iii*) to track polymerized MreB–YFP with time-lapse imaging, 0.003% xylose (5X) was used.

Single-Molecule Fluorescence Microscopy. Both white-light transmission and epifluorescence images of single molecules were acquired by using a Nikon TE300 inverted microscope. The general experimental arrangement is described in ref. 25; for full details, see *Supporting Text*.

To track fast- and slow-moving molecules, we used time-lapse imaging by placing a variable-length dark interval between exposure (integration) times. In cases of fast-moving molecules, such as monomeric MreB and cytoplasmic YFP, samples were illuminated with continuous laser light (no dark interval) with a 15.4-ms (65 Hz) integration time per frame. For slowly moving polymerized MreB, images were recorded with 9.9-s dark intervals (without laser illumination) between 100-ms exposures. Lastly, the fluorescence on-time distribution of polymerized MreB before photobleaching was measured with continuous irradiation and a 100-ms integration time.

Analysis of Motion. For the fast-moving molecules, the center of the spot in each image was determined manually, and an estimated diffusion coefficient for each single-molecule trajectory was computed by using the measured MSD for a 15.4-ms time lag. The resulting distributions of diffusion coefficients were compared with a theoretical distribution for observed D values, which takes into account the finite trajectory length (35).

For polymerized MreB, a 2D Gaussian function was fit to each single-molecule point-spread function to localize the position to $\pm$15 nm without pixelation error by using the MATLAB function FMINSEARCH. For measurements of positions as a function of time, we also tracked fixed quantum dots imbedded in the sample, which can be localized to $\pm$4 nm under our imaging conditions. To compensate for stage drifts during the time-lapse imaging, the positions of the MreB molecules were determined relative to the fixed quantum dot positions. The speed for a single trajectory was determined by the average of the interframe speeds for points along the trajectory.

For determinations of the velocity autocorrelation, molecules were tracked by hand to 1-pixel accuracy to extract the velocity $\vec{v}(t)$, and we used the expression $C_V(\tau) = \langle \vec{v}(t) \cdot \vec{v}(t + \tau) \rangle$, where $\langle\rangle$ indicates time average.

We thank Stefanie Nishimura for consultation regarding data analysis and Patrick McGrath for suggesting polar coordinates (r, θ) to analyze the direction of the polymerized MreB movements. This work was supported by Department of Energy Grant DE FG02-04ER63777 (to W.E.M.) and National Institutes of Health Grants 1P20-HG003638 (to W.E.M.), 2R01C-M051426 (to L.S.), and 2R01C-M032506 (to L.S.).

1. Bretschneider, T., Diez, S., Anderson, K., Heuser, J., Clarke, M., Müller-Taubenberger, A., Köhler, J. & Gerisch, G. (2004) *Curr. Biol.* **14,** 1–10.
2. Westphal, M., Jungbluth, A., Heidecker, M., Mühlbauer, B., Heizer, C., Schwartz, J., Marriott, G. & Gerisch, G. (1997) *Curr. Biol.* **7,** 176–183.
3. Pruyne, D. & Bretscher, A. (2000) *J. Cell Sci.* **113,** 571–585.
4. Møller-Jensen, J., Borch, J., Dam, M., Jensen, R. B., Roepstorff, P. & Gerdes, K. (2003) *Mol. Cell* **12,** 1477–1487.
5. Soufo, H. J. D. & Graumann, P. L. (2003) *Curr. Biol.* **13,** 1916–1920.
6. Kruse, T., Møller-Jensen, J., Løbner-Olesen, A. & Gerdes, K. (2003) *EMBO J.* **22,** 5283–5292.
7. Daniel, R. A. & Errington, J. (2003) *Cell* **113,** 767–776.
8. Gitai, Z., Dye, N. & Shapiro, L. (2004) *Proc. Natl. Acad. Sci. USA* **101,** 8643–8648.
9. Gitai, Z., Dye, N., Reisenauer, A., Wachi, M. & Shapiro, L. (2005) *Cell* **120,** 329–341.
10. Figge, R. M., Divakaruni, A. V. & Gober, J. W. (2004) *Mol. Microbiol.* **51,** 1321–1332.
11. Gitai, Z. (2005) *Cell* **120,** 577–586.
12. Pollard, T. D. & Mooseker, M. S. (1981) *J. Cell Biol.* **88,** 654–659.
13. Pollard, T. D. (1986) *J. Cell Biol.* **103,** 2747–2754.
14. Selve, N. & Wegner, A. (1986) *J. Mol. Biol.* **187,** 627–631.
15. Wang, Y. (1985) *J. Cell Biol.* **101,** 597–602.
16. Theriot, J. A. & Mitchison, T. J. (1991) *Nature* **352,** 126–131.
17. Rzadzinska, A. K., Schneider, M. E., Davies, C., Riordan, G. P. & Kachar, B. (2004) *J. Cell Biol.* **164,** 887–897.
18. Garner, E. C., Campbell, C. S. & Mullins, R. D. (2004) *Science* **306,** 1021–1025.
19. Desai, A. & Mitchison, T. J. (1997) *Annu. Rev. Cell Dev. Biol.* **13,** 83–117.
20. Esue, O., Cordero, M., Wirtz, D. & Tseng, Y. (2005) *J. Biol. Chem.* **280,** 2628–2635.
21. Esue, O., Wirtz, D. & Tseng, Y. (2006) *J. Bacteriol.* **188,** 968–976.
22. Carlier, M., Laurent, V., Santolini, J., Melki, R., Didry, D., Xia, G., Hong, Y., Chua, N. & Pantaloni, D. (1997) *J. Cell Biol.* **136,** 1307–1323.
23. Shapiro, L. (1976) *Annu. Rev. Microbiol.* **30,** 377–407.
24. Watanabe, N. & Mitchison, T. J. (2002) *Science* **295,** 1083–1086.
25. Deich, J., Judd, E. M., McAdams, H. H. & Moerner, W. E. (2004) *Proc. Natl. Acad. Sci. USA* **101,** 15921–15926.
26. Lommerse, P. H. M., Snaar-Jagalska, B. E., Spaink, H. P. & Schmidt, T. (2005) *J. Cell Biol.* **118,** 1799–1809.
27. Yu, J., Xiaojia, R., Lao, K. & Xie, X. S. (2006) *Science* **311,** 1600–1603.
28. Roberts, R. C., Toochinda, C., Avedissian, M., Baldini, R. L., Gomes, S. L. & Shapiro, L. (1996) *J. Bacteriol.* **178,** 1829–1841.
29. Dickson, R. M., Cubitt, A. B., Tsien, R. Y. & Moerner, W. E. (1997) *Nature* **388,** 355–358.
30. Harms, G. S., Cognet, L., Lommerse, P. H. M., Blab, G. A. & Schmidt, T. (2001) *Biophys. J.* **80,** 2396–2408.
31. Elowitz, M. B., Surette, M. G., Wolf, P. E., Stock, J. B. & Leibler, S. (1999) *J. Bacteriol.* **181,** 197–203.
32. Van Den Ent, E., Amos, L. A. & Lowe, J. (2001) *Nature* **413,** 39–44.
33. Iwai, N., Nagai, K. & Wachi, M. (2002) *Biosci. Biotechnol. Biochem.* **66,** 2658–2662.
34. Roeben, A., Kofler, C., Nagy, I., Nickell, S., Hartl, F. U. & Bracher, A. (2006) *J. Mol. Biol.* **358,** 145–156.
35. Vrljic, M., Nishimura, S. Y., Brasselet, S., Moerner, W. E. & McConnell, H. M. (2002) *Biophys. J.* **83,** 2681–2692.
36. Sheetz, M. P., Turney, S., Qian, H. & Elson, E. L. (1989) *Nature* **340,** 284–288.
37. Kusumi, A., Sako, Y. & Yamamoto, M. (1993) *Biophys. J.* **65,** 2021–2040.
38. Saxton, M. J. & Jacobson, K. (1997) *Annu. Rev. Biophys. Biomol. Struct.* **26,** 373–399.
39. Qian, H., Sheetz, M. P. & Elson, E. L. (1991) *Biophys. J.* **60,** 910–921.
40. Konopka, M. C. & Weisshaar, J. C. (2004) *J. Phys. Chem. A* **108,** 9814–9826.
41. Johns, L. M., Levitan, E. S., Shelden, E. A., Hotz, R. W. & Axelrod, D. (2001) *J. Cell Biol.* **153,** 177–190.
42. Paavilainen, V. O., Bertling, E., Falck, S. & Lappalainen, P. (2004) *Trends Cell Biol.* **14,** 386–394.
43. Fujiwara, I., Takahashi, S., Tadakuma, H., Funatsu, T. & Ishiwata, S. (2003) *Nat. Cell Biol.* **4,** 666–673.
44. Jones, L. J. F., Carballido-Lopez, R. & Errington, J. (2001) *Cell* **104,** 913–922.
45. Soufo, H. J. D. & Graumann, P. L. (2004) *EMBO Rep.* **5,** 789–794.
46. Nilsen, T., Yan, A. W., Gale, G. & Goldberg, M. B. (2005) *J. Bacteriol.* **187,** 6187–6196.
47. Kruse, T., Blagoev, B., Løbner-Olesen, A., Wachi, M., Sasaki, K., Iwai, N., Mann, M. & Gerdes, K. (2006) *Genes Dev.* **20,** 113–124.
48. Carballido-Lopez, R. (2003) *Dev. Cell* **4,** 19–28.
49. Shih, Y. L., Le, T. & Rothfield, L. (2003) *Proc. Natl. Acad. Sci. USA* **100,** 7865–7870.
50. Meisenzahl, A. C., Shapiro, L. & Jenal, U. (1997) *J. Bacteriol.* **179,** 592–600.
51. Ely, B. (1991) *Methods Enzymol.* **204,** 372–384.